IEEE Access
Multidisciplinary ⋮ Rapid Review ⋮ Open Access Journal

Received 10 May 2024, accepted 20 May 2024, date of publication 24 May 2024, date of current version 3 June 2024.

Digital Object Identifier 10.1109/ACCESS.2024.3405176

RESEARCH ARTICLE

Dynamic Power Flow Modeling Primary and Secondary Frequency Regulations

ROBERTO BENATO, (Senior Member, IEEE), GIOVANNI GARDAN, (Member, IEEE), AND FRANCESCO SANNITI, (Member, IEEE)

Department of Industrial Engineering, University of Padova, 35131 Padua, Italy

Corresponding author: Giovanni Gardan (giovanni.gardan@phd.unipd.it)

ABSTRACT In power systems, the steady-state operations following any disturbance can be assessed by means of time-domain simulations, which consider the dynamic of the system without simplifying hypotheses. This paper proposes a formulation of the power flow problem with distributed slack bus model able to determine the steady-state impact on frequency and generation set-points of primary and secondary frequency regulation. This is done by deriving the real power balance expressions (including power losses, primary/secondary regulation, and the real frequency deviation) before and after the occurrence of any event or disturbance. This is achieved without resorting to the solution of a time-domain simulation. The performance of the proposed formulation is discussed through the standard WSCC 9-bus system and a 102-bus model of the Sicilian grid. Solutions are compared with those obtained with conventional time-domain simulations.

INDEX TERMS Dynamic power flow, distributed slack bus, primary frequency regulation, secondary frequency regulation.

A. SETS AND INDICES

$\cdot*$	Steady-state initial regime.
$\cdot'$	Steady-state value after PFR.
$\cdot''$	Steady-state value after PFR + SFR.
I	Set of generators providing PFR.
II	Set of generators providing PFR & SFR.
slk	Slack-bus

B. SYMBOLS

Δp_g	Power increment of the generator g [MW].
k'_g	Generator PFC [MW/Hz].
k_U	Load PFC [MW/Hz].
K'	Sum of all generator and load PFC [MW/Hz].
Δf	Steady-state frequency deviation [Hz].
Δp	Disturbance [MW].
p_g	Active power of the generator g [MW].
p_{loss}	Network Losses [MW].
p_{L}	Active power of the generator g [MW].
f	Network frequency [MW].
$k''g$	Secondary control reserve [MW].
K''	Sum of all secondary control reserve [MW].
ΔL	SFR Signal level [MW].
σ	Frequency droop constant [*adimen.*].

C. ACRONYMS

PF	Power Flow.
DSB	Distributed Slack Bus.
PFR	Primary Frequency Regulation.
PFC	Power Frequency Characteristic.
SFR	Secondary Frequency Regulation.
PFPD-D	Dynamic Power Flow of University of Padova.
AGC	Automatic Generation Control.
TDS	Time Domain Simulation.
QSS	Quasi Steady-State.
vRES	Variable Renewable Energy Sources.
TSO	Transmission System Operator

The associate editor coordinating the review of this manuscript and approving it for publication was Salvatore Favuzza.

I. INTRODUCTION

A. MOTIVATIONS

In the classical power flow formulation, any power unbalance between generators and loads (including power losses) is allocated to a single generator, which serves as slack bus. However, this mathematical artifice is not consistent with the actual behavior of the system and could bring to misleading results in the study of steady-state planning and operation analyses. In real power systems, in fact, all synchronous machines vary their power production, following a power unbalance, by means of their primary and secondary frequency controllers.

In technical literature, this fact encouraged the development of Distributed Slack Bus (DSB) model, which distributes the power unbalances to different generators participating to a centralized regulation process. The main limitation of these approaches is that the exact coefficients related to the contribution of each generator Δp_g cannot be determined *a priori*, since they are weighted by the Power Frequency Characteristic (PFC), k'_g, and by the secondary control reserve, k''_g, so by the steady-state frequency deviation Δf and the SFR Signal level ΔL reached after the actions of PFR and SFR, by the well-known relations (1):

$$\begin{aligned} \Delta p'_g &= k'_g \Delta f; \\ \Delta p''_g &= k''_g \Delta L; \end{aligned} \tag{1}$$

However, Δf and ΔL depend on the PFR and SFR contributions themselves. To overcome this limitation, Δf and ΔL are typically estimated by the two following well-known relations given by [1]:

$$\Delta f = \frac{\Delta p}{K'}; \ \Delta L = \frac{\Delta p}{K''} \tag{2}$$

where K'[MW/Hz] is the sum of all the PFC of the generators participating to the PFR and of the load, K''[MW] is the sum of all secondary control reserves, and Δp is the active power perturbation.

However, the approximation (2) does not consider the actual new steady-state regimes derived from the actions of PFR and SFR. After these actions, indeed, a new allocation of the active power between the generators, considering also new power losses, should be considered, but it is neglected by (2). The new system power losses, after a frequency disturbance, in fact, have non-negligible impact on the contribution of each single generator output. Therefore, simple application of (2) could bring to a misleading consideration of the new active power set-point of the generators involved in the PFR, especially in large networks.

To overcome the above-mentioned approximation, it is proposed a simple and accurate framework (PFPD-D) computing the power flow solution after the occurrence of a disturbance. Such formulations could be meaningful for design and planning, predicting the effect of the regulators acting after a disturbance, without exploiting time domain simulations or complex formulations. Such disturbances (load/generator shedding, line tripping, etc.) are the ones occurring in real power systems and are increasingly frequent with the vRES integration, characterized by intermittent generation [2].

B. LITERATURE REVIEW

In 1986, the first contribution introducing the concept of dynamic power flow was presented in [3] being based on the DSB model [4]. The dynamic power flow models [2], [3], [5], [6], [7], [8], [9] consist in distributing any power unbalances, after the occurrence of a disturbance, among all the generators, by considering the frequency deviation inside the model.

Therefore, it radically differs from the classical power flow problem [10], [11], [12], where the power balance is restored by the slack generator only, so bringing to unreliable solutions especially for large power systems, as remarked in [13] and [14].

Regarding the commercial software solutions proposed for the dynamic power flow, some software considers different approaches to balance the power difference between the supplied and dispatch power, *i.e.*, according to primary control [15]. However, these methods introduce some simplifying hypotheses, *e.g.,* exploiting the first expression of (2) to compute the dispatch power of new steady-state regime after disturbances.

To address the problem of distributing the incremental powers after the occurrence of disturbance, some contributions propose different criteria. In [3] and [16], the generator power mismatches implicitly contain the presence of the frequency deviation. In [17], participation factors are obtained by considering the costs of generating units, thus, implementing an economic dispatch of the power unbalance. References [18] and [19] propose to distribute the power unbalance within each generator considering the contribution of the Primary Frequency Regulation (PFR).

From a practical standpoint, the dynamic power flow problem is becoming important today, due to increasing presence of vRES in power systems. In [2], [8], and [9] a stochastic approach to dynamic power flow is proposed, considering the PFR uncertainties in networks with high vRES penetration. In [7], an iterative dynamic power flow model attempts to update the power flow solutions based on PFR in presence of high wind generation. However, these formulations consider only the PFR, without exploiting the capability of generators to also perform SFR.

Alternatively, instead of using dynamic power flow techniques, long-term responses to power system disturbance can be modelled by means of the Quasi Steady-State (QSS) approaches [20], [21], [22], which simulate power system time evolution by means of a sequence of equilibrium steady-state points. However, such methods start from the complete dynamic model to derive the QSS approximations, differently from the dynamic power flows, as the one proposed in this paper (see Sect. I-C). Indeed, dynamic power flow methods must not be confused with the dynamized power flow methods lately developed to trace the power flow solutions by

means of differential transformation, simulating the network dynamic evolution [23], [24], [25]. These algorithms [23], [24], [25], in fact, simplify the mathematical treatment of time-domain analysis but do not give a practical tool to forecast the real impact of the PFR and SFR on the steady-state power flow problem.

C. CONTRIBUTIONS

This paper proposes an alternative theoretical framework considering the action of dynamic processes, but inside a new steady-state algorithm (PFPD-D).

PFPD-D is made of two simple outer-loop iterative methods (named as ''Method A'' and ''Method B'') computing the steady-state regimes after the actions of PFR and SFR (*i.e.*, the regulations happening after any network disturbance as load/generator shedding, line tripping, *etc.*). These outer-loop iteratively solves the classical power flow problem in which the new system power losses, the new frequency deviations, the new secondary regulation signal levels, and so the new contribution Δp_g to be assigned to each generator are updated till exact convergence values.

These iterative procedures allow considering the precise impact of PFR and SFR without recurring to model simplifications as in (2), QSS simulations, and Time Domain Simulations (TDSs). The steady-state results of PFPD-D, however, are consistent with the final values obtained with time domain integration of the fully-fledged dynamic model of the system.

Indeed, it is important to highlight that this paper does not give any information about the dynamic evolution of the system after the disturbance. The iteration sequence is not representative of different power flow solutions over the time after the disturbance, instead it represents the iterative steps necessary to reach the convergence criterion of the algorithm (see Sect. II-A and II-B).

Section II-A describes the theoretical passages to find the ''Method A'' algorithm of PFPD-D, whereas in Sect. II-B the ''Method B'' algorithm of PFPD-D is explained. In sect. III-A simulation results of PFPD-D in the standard WSCC 9-bus system are applied, in sect. III-B, instead, results of PFPD-D are proposed in a real power system data, *i.e.*, the Sicilian power system (102 buses).

II. INCLUDING FREQUENCY REGULATION WITHIN PF SOLVERS

In this section, the development of two iterative algorithms that find the steady-state solutions after the action of PFR (see Sect. II-A) and PFR+SFR (see Sect. II-B) following a power disturbance is presented. The formulations are derived by merging the classical power flow equations with the static characteristics of PFR and SFR regulators.

A. PRIMARY FREQUENCY REGULATION (METHOD A)

The active power balance in steady state, with the inclusion of the power losses, can be written as:

$$\sum p_g^* = \sum p_L^* + p_{loss}^* \tag{3}$$

where Σp_g^* is the sum of the generated active power; Σp_L^* is the sum of the power absorbed by the load and p_{loss}^* are the network losses (they depend on the power flow solution).

Let now assume that a disturbance, Δp, occurs: if f^* is the pre-disturbance frequency value, the steady-state frequency after the action of PFR is:

$$f = f^* + \Delta f \tag{4}$$

In this condition, generator g injects the following active power, by considering its PFC k_g:

$$p_g' = p_g^* - k_g \Delta f \tag{5}$$

and the overall network power balance after the occurrence of the disturbance is:

$$\sum p_g^* - \sum k_g \Delta f = \left(\sum p_L^* + \sum k_U \Delta f\right) + p_{loss}' - \Delta \mathrm{p} \tag{6}$$

where k_U is the PFC of the load. By including (3) into (6), it yields:

$$\begin{aligned} &\left(\sum p_L^* + p_{loss}^*\right) - \sum k_g \Delta f \\ &\quad = -\Delta p + \left(\sum p_L^* + \sum k_U \Delta f\right) + p_{loss}' \end{aligned} \tag{7}$$

Defining $K = \sum k_g + \sum k_U$, (7) becomes:

$$p_{loss}^* - K \Delta f = -\Delta p + p_{loss}' \tag{8}$$

The expression of Δf can be derived by knowing the disturbance Δp and the power losses before the disturbance and after the action of the PFR:

$$\Delta f = \frac{\Delta p + p_{loss}^*}{K} - \frac{p_{loss}'}{K} \tag{9}$$

The first expression on the right side is a constant term and the second expression depends on the power losses p_{loss}' after the primary frequency regulation: by naming A the constant term, (9) can be written as:

$$\Delta f = A - \frac{p_{loss}'}{K} \tag{10}$$

Since the final steady-state regime after the action of PFR is unknown, so it is p_{loss}', to compute Δf an iterative scheme must be set.

Fig. 1 shows the flow chart of the proposed algorithm computing the new steady state regime, after the action of the PFC distributed between the generators. The input data are the steady-state conditions of the network before the disturbance, Δp: the set of the power generated p_g^*, the power losses p_{loss}^*, and the K coefficient for PFC. Then, an initial Δf=A is set to compute the initial guess of the generator active power. Thus, a new power flow is computed so giving a new value for the losses $p_{loss}^{(n)}$ which can be exploited to update Δf by (9). As shown in Fig. 1, the procedure must be iterated till convergence, *i.e.*, the difference between two consecutive frequency deviation settles at a constant value:

$$|\Delta f^{(n)} - \Delta f^{(n-1)}| < tol.$$

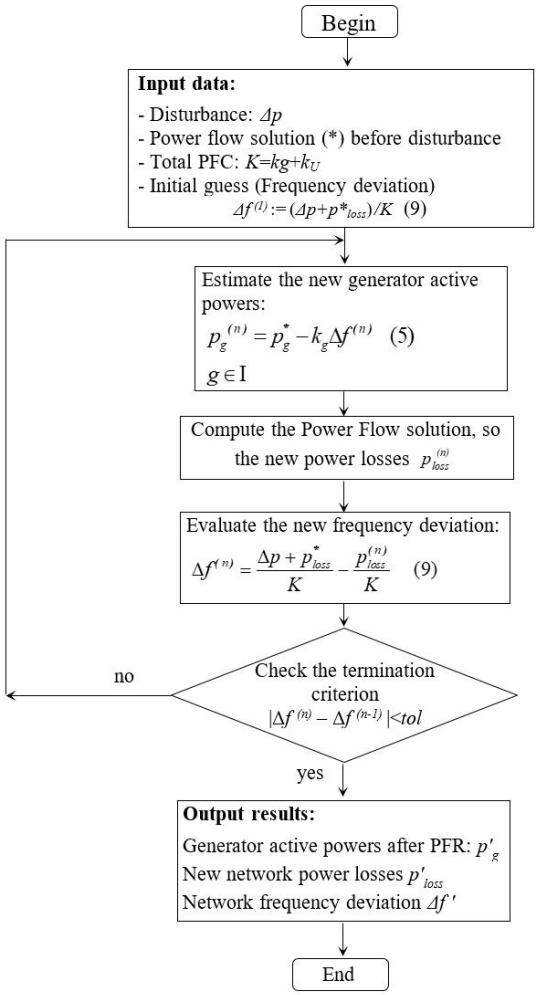

FIGURE 1. Flow chart of the proposed iterative scheme computing the power flow solution for Method A.

It is worth noting that each power flow inside the iterative cycle must consider the generator power injection computed with the updated frequency, $f = f^* + \Delta f$.

The algorithm output gives the steady-state regime settling after a disturbance and after the PFR action, *i.e.*, the new $\Delta f'$, p'_{loss}, p'_g. Note that the results are found without considering neither simplifying hypotheses nor dynamic simulations.

B. PRIMARY AND SECONDARY FREQUENCY REGULATION (METHOD B)

A similar procedure to derive Δf can be applied to compute the steady-state condition after the PFR and the Secondary Frequency Regulation (SFR). In this case, two groups of generators should be identified: the ones performing the PFR service only (I) and the ones also performing the SFR service (II).

The balance (3) happening before the disturbance, Δp, can be rewritten as:

$$\sum p_g^* = \sum_{g\in \mathrm{I}} p_g^* + \sum_{g\in \mathrm{II}} p_g^* = \sum p_L^* + p_{loss}^* \qquad (11)$$

The SFR perfectly tracks the frequency to restore the pre-disturbance frequency value f^*, so each generator reacts to the frequency deviation $-\Delta f$ by restoring the pre-contingency power output p_g^* according to the static power-frequency PFR curve of each generator.

The generators providing the PFR + SFR produce an incremental power with respect to the pre-contingency condition, so that their total contribution can be written as:

$$\sum_{\mathrm{II}} p_g'' = \sum_{\mathrm{II}} p_g^* + \sum_{\mathrm{II}} k_g'' \Delta L \qquad (12)$$

where ΔL represents a level signal sent to all generators by the central dispatch control and k_g'' are the weight coefficients determining the power share to be provided with the SFR.

The level signal ΔL is a constant value for all the generators participating to the SFR. Note that ΔL is a value which could be important from a power dispatch standpoint: it forecasts the power share that each generator should provide to restore the pre-contingency frequency. Therefore, (12) gives the power share which can be computed with time domain simulation implementing Automatic Generation Controls (AGCs).

In these conditions, the complete power balance after the SFR service is given by:

$$\left(\sum_{\mathrm{I}} p_g^* + \sum_{\mathrm{II}} p_g^*\right) + \sum k_g'' \Delta L = -\Delta p + \sum p_L^* + p_{loss}'' \qquad (13)$$

Defining $K'' = \sum k_g''$, the expression of ΔL can be derived as it follows:

$$\Delta L = \frac{-\Delta p - p_{loss}^*}{K''} + \frac{p_{loss}''}{K''} = B + \frac{p_{loss}''}{K''} \qquad (14)$$

where the term on the right side of the expression is constant and has been called B. It is worth noting the analogies in the approach proposed in Sect. II-A.

Similarly to the PFR procedure, the final expression of ΔL can be computed starting from $\Delta L = B$ and updating ΔL based on the power losses obtainable with power flow solutions computed iteratively. Fig. 2 shows the flow chart of the proposed algorithm computing the new steady state regime, after the action of the SFR of the generators providing the secondary reserve service.

The input data are the entities of the disturbance, Δp, the set of the power generated p_g^*, the power losses p_{loss}^*, and the K'' coefficient for SFC. Then, an initial $\Delta L = B$ is set to compute the initial guess of the generator active power (see Fig. 2). Thus, a new power flow is computed so giving a new value for the losses $p_{loss}^{(n)}$ which can be exploited to update ΔL by (14).

As shown in Fig. 2, the procedure must be iterated till convergence, *i.e.*, the difference between two consecutive signal deviation settles at a constant value:

$$|\Delta L^{(n)} - \Delta L^{(n-1)}| < tol$$

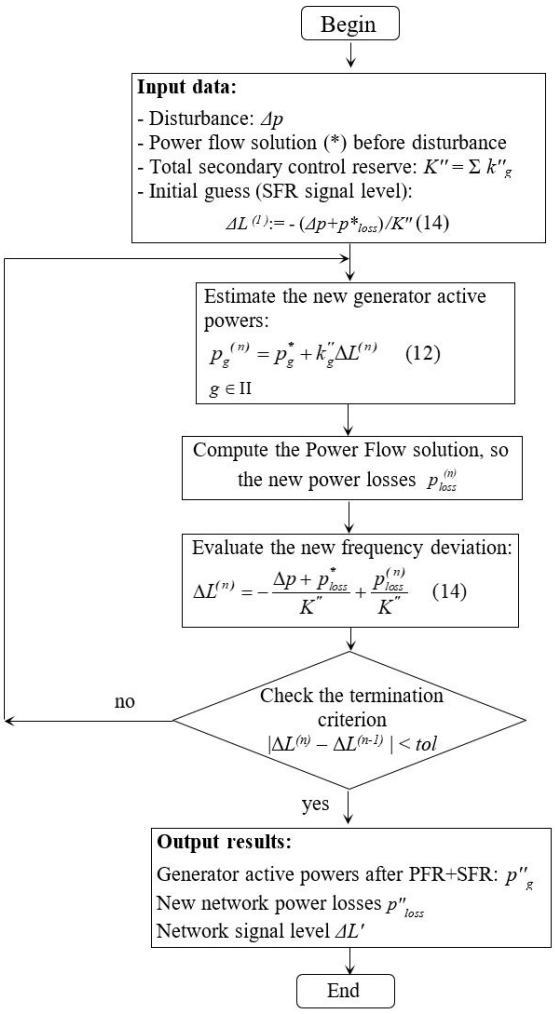

FIGURE 2. Flow chart of the proposed iterative scheme computing the power flow solution for Method B.

Again, the output of the new steady-state regime occurring after a disturbance and the regulation of the PFR+SFR can be found (*i.e.*, the signal level ΔL, p''_{loss}, p''_g) without simplifying hypotheses and without recurring on dynamic simulations.

It is worth noting that, in this case, PFR and SFR act simultaneously. The action of the PFR is implicitly included in the procedure but no operating point related to the PFR is derived. In fact, the steady-state operating point reached after the SFR action is independent from the PFR behaviour. Indeed, input variables of this procedure depend only on pre-disturbance parameters, and not on intermediate parameters resulting from the calculation with only PFR derived in Section II-A.

III. SIMULATION RESULTS

The algorithm **PFPD-D** is applied to the WSCC 9-bus system and to a real-world grid model, namely, the Sicilian transmission system (102-bus system). The WSCC 9-bus network is chosen, since it is a well-recognized benchmark for power system simulations developed by Anderson and Fouad [26]. The 102-bus Sicilian network, instead, is chosen since it is significative large and real power system. This network contains also the connection with the power system of the Malta island [27]. So, the effectiveness of **PFPD-D** is also tested by a real-world power system.

The results of **PFPD-D** are always compared with a conventional time domain simulation. In fact, time domain simulations give the steady-state value settling at the end of the transients following any disturbance and the actions of both PFR and SFR.

For the simulations of Method A, the comparison between the results obtained considering the frequency deviation of **PFPD-D** proposed in (10), the steady-state approximation of (2) and the results of TDSs performed with Dome [28] is performed. Dome is a recognized power system analysis software written in Python, C and Fortran and developed by Prof. Milano. Its distinguishing feature relies on its usability by the interested researchers, who can contribute to improve its modular structure for the sake of power system community.

For the Method B simulations, the comparison between the new active power injected by the generators obtained by (12) and the results of TDS performed with Dome is carried out.

A. CASE STUDY I: THE WSCC 9-BUS SYSTEM

The scheme of the WSCC 9-bus system adopted for the simulations is shown in Fig. 3. It is supposed that each generator provides both the PFR and SFR service.

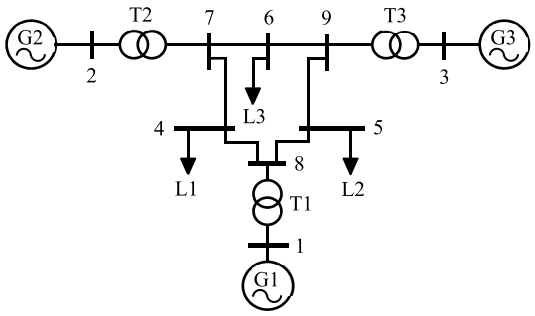

FIGURE 3. WSCC 9-bus test system.

For PFR, a PFC value of 50 MW/Hz (which corresponds to a droop constant σ =0.04 weighted on 100 MVA power base) is set. For SFR, a value of 100 MW for all the k''_g coefficients of all the generators is set. The base-case total dispatched power is 319.65 MW.

Table 1 shows the frequency deviation and the active powers generated in steady state considering PFR and after a loss of load of Δp =9.6 MW (3% of the total generated power). Such results are performed by considering Method A (see Sect. II-A). The standard formulation (2) introduces an error respect to TDS for the frequency estimation of 3.77%; differently, PFPD-D estimation is more in tune with

TABLE 1. Results of the comparison for the 9-bus case. The percentage values are computed with respect to the frequency and power mismatch between pre and post disturbance.

	Pre-disturbance	Standard (2)	PFPD-D	Dynamic model (TDS)	% error TDS - (2)	% error TDS - PFPD_D
Δf [Hz]	0	0.0639	0.0662	0.0664	3.77 %	0.30 %
p_{G1} [MW]	71.65	68.12	68.34	68.32	6.01 %	0.60 %
p_{G2} [MW]	163.00	159.80	159.70	159.68	3.61 %	0.60 %
p_{G3} [MW]	85.00	81.80	81.70	81.68	3.61 %	0.60 %

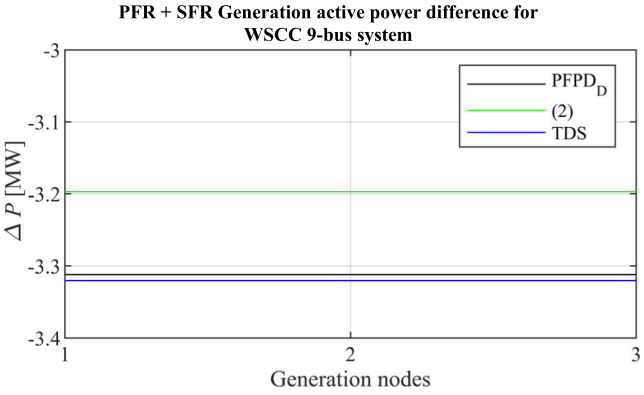

FIGURE 4. Steady-state generation power difference computing Method B for the WSCC 9-bus system.

the dynamic simulation, with an error of 0.30% with respect to TDS (see Tab. 1). Moreover, the errors in the power deviation post-disturbance and after the action of the PFR always remain below 1% for PFPD-D. Differently, the corresponding errors for standard formulation (2) reach the value 6%. This confirms that PFPD-D is more in tune with TDS, so better matching the network reality (see Tab. 1).

By considering Method B, Fig. 4 shows the difference between steady-state active power generated before and after the action of the SFR for the WSCC 9-bus system. All the coefficients k_g'' are constant, so the same active power difference is injected by generators. Fig. 4 highlights a generator active power difference between PFPD-D and TDS of 0.30% and between PFPD-D and the analytical formulation (2) of 3.6%.

B. CASE STUDY II: THE SICILIAN GRID (102-BUS MODEL POWER SYSTEM)

Next, we consider a 102-bus model of the Sicilian grid, see Fig. 5. In this case, the disturbance is a 34.5 MW loss of load (3% of the total generated power) in the Malta island (see "Location 4" in Fig. 5).

The total pre-disturbance dispatched power is 1150 MW.

In this case, all generators participate to the PFR service with a PFC of 50 MW/Hz. In fact, since this network is part of the Italian transmission system, the participation of all its generators is mandatory. According to the Italian grid code [29], indeed, all the generation units with nominal power higher

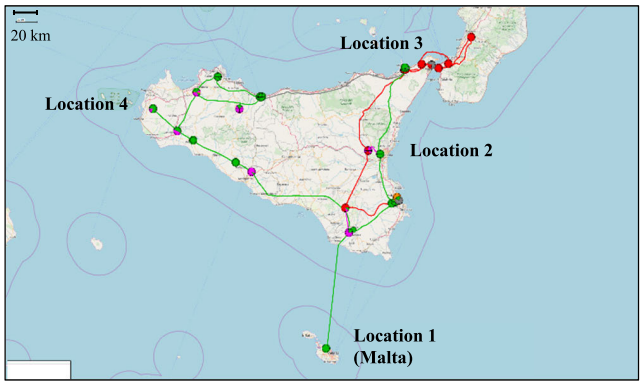

FIGURE 5. Sicilian transmission network.

than 10 MVA must provide PFR service. However, PFPD-D is completely general, so the case where some generators do not provide PFR can be easily handled by fixing a PFC equal to 0 MW/Hz.

The results of the comparison are reported in Table 2 in terms of frequency deviation and active and reactive power provided by the slack bus. Such results are performed by considering only PFR (see Sect. II-A). In this case, the frequency estimation error introduced by the standard formulation (2) is 4.5%, whereas PFPD-D estimates the real frequency deviation with an error of 0.39%.

Regarding the estimation of the active power deviations, Tab. 2 shows that the errors of PFPD-D respect to the real dynamic TDS are always below 1 %, instead the errors between (2) and TDS, in some cases, reach 4.8 % of deviation. In Fig. 6, the comparison in terms of active power provided by all other generators computing Method A is shown.

Fig. 6 confirms that the error observed in the frequency estimation by (2) propagates itself also in the active power generated by each generator after the action of the PFR, as already shown in Tab. 2. Contrarily, the estimation made by PFPD-D returns errors always below 1%.

By considering Method B, Fig. 7 shows the difference between steady-state active power generated before and after the action of PFR + SFR for the Sicilian network. All the coefficients k_g'' are constant, so that the same active power difference is injected by generators.

Fig. 6 highlights that the generator active power difference between PFPD-D and TDS is 0.35% for the Sicilian network.

C. DISCUSSION ON THE CONVERGENCE OF PFPD-D

Since Method A and Method B are iterative algorithms (see Sect. II-A and II-B), the problem related to their convergence properties must be addressed.

Method A and Method B are outer loops computing the power flow problem (internal loop) iteratively. Thus, if the network under analysis is well conditioned, convergence is guaranteed as long as the power flow convergence is guaranteed. Moreover, several tests show that if the entity of the disturbance is too heavy, *e.g.*, loss of a big amount of load centers or generation units, the power flow problem

TABLE 2. Comparative results for the Sicilian grid. The percentage values are computed with respect to the frequency and power mismatch between pre and post disturbance.

	Pre-disturbance	Standard (2)	PFPD-D	Dynamic model (TDS)	% error TDS - (2)	% error TDS - PFPD_D
Δf [Hz]	0	0.0493	0.0514	0.0516	4.5%	0.39 %
p_{G1} [MW]	275.64	273.01	273.07	273.05	0.02 %	0.52 %
p_{G2} [MW]	65.40	62.94	62.83	62.82	0.21 %	0.02 %
p_{G3} [MW]	67.00	64.54	64.43	64.42	0.22 %	0.02 %
p_{G4} [MW]	47.40	44.94	44.83	44.82	0.30 %	0.02 %
p_{G5} [MW]	61.70	59.24	59.13	59.12	0.21 %	0.02 %
p_{G6} [MW]	61.50	59.04	58.93	58.92	0.21 %	0.02 %
p_{G7} [MW]	0	-2.46	-2.57	-2.58	4.8 %	0.40 %
p_{G8} [MW]	71.20	68.74	68.63	68.62	0.12 %	0.02 %
p_{G9} [MW]	131.50	129.04	128.93	128.91	0.10 %	0.01 %
p_{G10} [MW]	62.50	60.04	59.93	59.92	0.21 %	0.01 %
p_{G11} [MW]	0	-2.46	-2.57	-2.58	4.82 %	0.40 %
p_{G12} [MW]	66.20	63.74	63.63	63.62	0.20 %	0.02 %
p_{G13} [MW]	163.40	160.94	160.83	160.82	0.10 %	0.01 %
p_{G14} [MW]	73.20	70.74	70.63	70.62	0.18 %	0.02 %

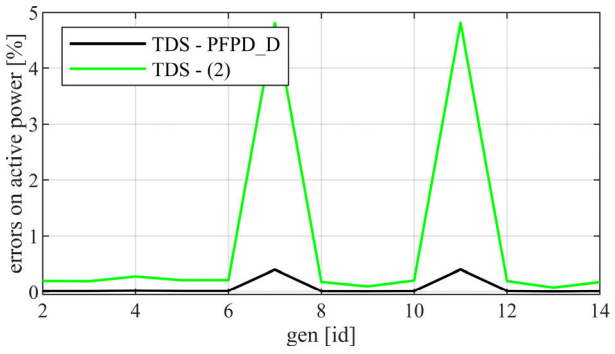

FIGURE 6. Percentage errors between TDS and PFPD-D and between TDS and (2) for the active power provided by all generators for Method A in the Sicily network (102-bus system).

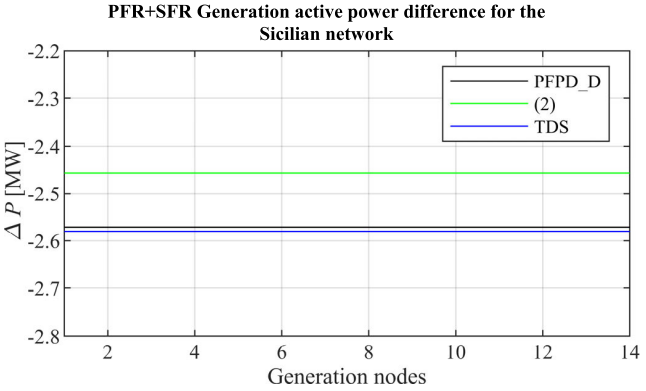

FIGURE 7. Steady-state generation power difference computing Method B for the Sicilian network.

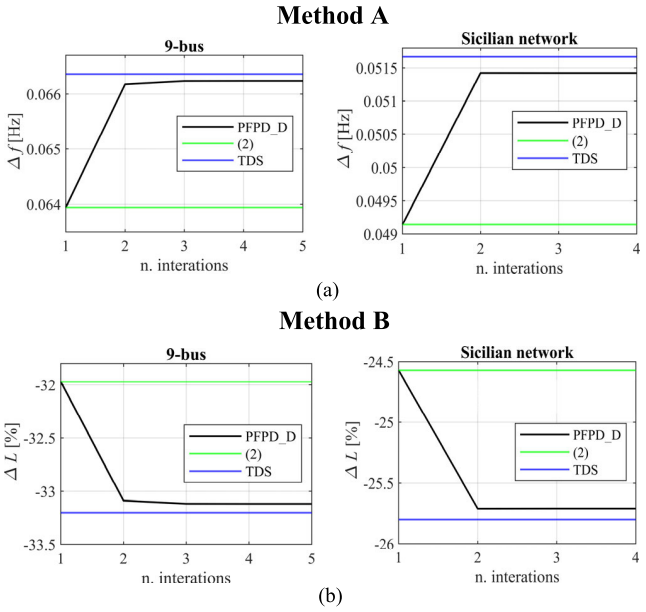

FIGURE 8. Convergence trend of PFR (Method A) and for PFR+SFR (Method B) for the WSCC 9-bus system (a) and for the Sicilian network (102-bus system) (b).

remains well-conditioned. This because before the power flow computation, the reassignment of the generation outputs (see (5) for Method A, and see (12) for Method B) restores the absorbed/generated power balance.

Though any power flow solver could be used for PFPD-D, in this work, we implement the proposed technique using the PFPD solver described in [30]. This choice comes from its convergence robustness and good computational performances [30].

By considering the 9-bus case and the Sicilian network case, the convergence trend of Methods A is shown in Fig. 8a (frequency tolerance of 10^{-6} Hz): the method converges in 5 iterations with a CPU-time of 70 ms for the WSCC 9-bus network, and with 4 iterations with a CPU-time of 80 ms for the Sicilian network. For each grid, the error of the approximate solution falls below 1% after the first iteration.

Similarly to Method A, the convergence trend of Method B for the 9-bus case and the Sicilian network case, is shown in Fig. 8b (signal level tolerance of 10^{-6} Hz). The method converges in 4 iterations with a CPU-time of 70 ms for the WSCC 9-bus network, and with 4 iterations with a CPU-time of 80 ms for the Sicilian network. Also in this case, for each grid, the error of the approximate solution falls below 1% after the first iteration. Please note the CPU times for both Method A and B are the same, since the two iterative methods have the same structure.

The method allows accurately calculating the frequency deviation value after the second iteration for both cases. Fig. 9 shows the convergence speed of the iterative method.

TABLE 3. Comparative results for the Sicilian grid by varying the disturbance entity and location.

Disturbance Entity	Location 1		Location 2		Location 3		Location 4	
[%] respect to the total load	TDS- (2) % error on Δf	TDS - PFPD-D % error on Δf	TDS- (2) % error on Δf	TDS - PFPD-D % error on Δf	TDS- (2) % error on Δf	TDS - PFPD-D % error on Δf	TDS- (2) % error on Δf	TDS - PFPD-D % error on Δf
2.5	4.92	0.40	0.67	0.23	0.87	0.70	2.31	0.15
5	4.40	0.39	0.59	0.23	0.77	0.69	2.10	0.14
7.5	3.89	0.39	0.50	0.23	0.68	0.69	1.87	0.14
10	3.38	0.34	0.42	0.23	0.57	0.68	1.65	0.13

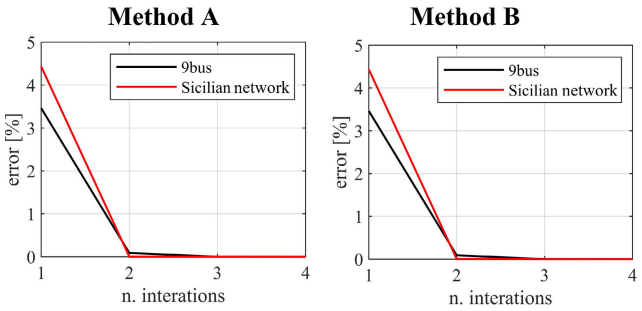

FIGURE 9. Convergence speed of Method A and Method B applied to the 9-bus network and to the Sicilian network (102-bus system).

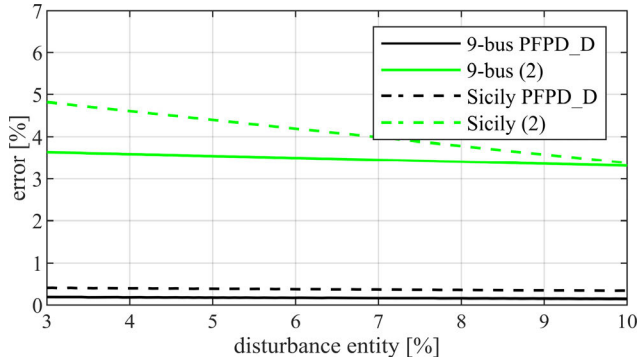

FIGURE 10. Frequency deviation percentage error between PFPD_D and TDS (black lines) and between (2) and TDS (grey lines) by varying the power disturbance entity with Method A.

With the aim of verifying the robustness of PFPD-D algorithm, two parametric analyses are performed: the first by changing the entity of the disturbance (see Fig. 10) and the second by changing the PFC of all generators (see Fig. 11). The results given by PFPD_D and by formulation (2) are compared with the results of the complete TDS in terms of percentage errors. Fig. 10 shows the results of the parametric analysis by varying the disturbance entity. The percentage error in the frequency deviation estimation of the formulation (2) increases with the decreasing of the disturbance entity, and it remains always above 3% for each grid under analysis. However, the error between PFPD_D and TDS remains below 1% regardless of the entity of the disturbance.

Fig. 11 shows the results of the parametric analysis by varying the PFC of each generator. In this case, the percentage error in the frequency deviation estimation does not depend

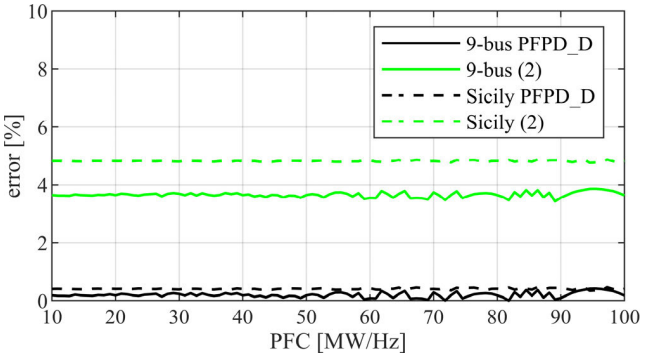

FIGURE 11. Percentage error between PFPD_D and TDS (black lines) and between (2) and TDS (grey lines) by varying the PFC of each generator.

on the generator PFC and it remains always close to 4% with the classical formulation (2) but it decreases under 0.5% with the PFPD-D algorithm. The actual minimum error is reached for a PFC value of 88 MW/Hz.

These important results suggest that the frequency estimation given by (2), and the derived PFR contributions of the generators, are less accurate chiefly for small disturbance, which is the situation in which they have the biggest impact, *i.e.*, in the economic dispatch for the allocation of ancillary services. Otherwise, the proposed procedure allows to strongly improve the accuracy in a simple and effortless way.

Eventually, Table 3 presents the results for the Sicilian grid of a parametric analysis performed by changing the disturbance entity and the location of the disturbance (for the locations of the disturbances refer to the geographic maps in Fig. 5).

The percentage error between PFPD_D and TDS for the frequency deviation is always below 1%, whatever the location of the disturbance is. Differently, the errors obtained with (2), especially for Location 1 and Location 4, are non-negligible and close to 5%.

IV. CONCLUSION

A novel dynamic power flow, named PFPD-D, is proposed in the paper. This algorithm is made of two iterative methods (Method A and Method B) giving the steady-state solutions after the occurrence of a power system disturbance. PFPD-D method does not use neither any simplifying hypotheses nor QSS/TDS in the computation of the frequency deviations. In fact, the steady-state effects of the system control devices

(primary and secondary regulators), the impact of frequency variations, and the impact on the system of the new power losses are considered without resorting to the whole system of differential algebraic equations describing the power system dynamic. Moreover, an evaluation of the power system signal level useful for a centralized secondary regulation of power system is performed in the paper. The high convergence speed of PFPD-D, together with its accuracy, makes PFPD-D preferable to time-domain simulations for planning and operation analyses.

The paper shows that the frequency deviations and the power losses, computed by means of these new formulations, are in tune with the exact solution of the dynamic model both for a reference network and for a model of the Sicilian grid. Simulation results also show that the well-known distributed slack-bus formula (2), typically used to estimate the steady-state frequency deviation, could differ from the exact solution up to 6 %.

The advantages of PFPD-D are the ease of implementation, together with the precision of the results without resorting to the high computational cost of time domain simulations. However, only the steady-state operating points after the actions of PFR and SFR can be estimated. This paper is suggested for power system planners and designers involved in assessing the power system robustness and stability after the occurrence of any disturbance.

Further researches are ongoing to assess the applicability of PFPD-D to real and large power systems (*e.g.*, the Italian transmission power system and the ENTSO-E power system).

A. APPENDIX A

Data of the WSCC 9-bus system of Fig. 3 are presented in this appendix, being classified in Bus data (Tab. 4), Transformer data (Tab. 5), and Line data (Tab. 6). Regarding the Sicilian network shown in Fig. 4, its data cannot be published due to non-disclosure agreements with the Italian TSO Terna. Tab. 7 shows some aggregated data about the Sicilian network. Both networks are operated at the European industrial frequency of 50 Hz.

TABLE 4. WSCC 9-bus system: bus data.

Bus ID	Type	P [MW]	Q [Mvar]	$V_{nominal}$ [kV]
1	Slack	-	-	16.5
2	PV	265	-	18.0
3	PV	260	-	13.8
4	PQ	125	50	230
5	PQ	150	30	230
6	PQ	100	35	230
7	PQ	0	0	230
8	PQ	0	0	380
9	PQ	0	0	380

(*) P is the active power injected (for PV buses) or absorbed (for PQ buses), Q is the reactive power injected (for PV buses) or absorbed (for PQ buses)

TABLE 5. WSCC 9-bus system: transformer data.

Transf. ID	Sending bus	Receiving bus	Sending voltage [kV]	Receiving voltage [kV]	Vcc [%]	Pcc [%]	P_{nom} [MW]
1	1	8	16.5	230	5.76	0	100
2	2	7	18.0	230	6.25	0	100
3	3	9	13.8	230	5.86	0	100

(*) Vcc is the percentage short-circuit voltage, Pcc is the percentage short-circuit power, P_{nom} is the transformer nominal power.

TABLE 6. WSCC 9-bus system: line data.

Line ID	S end	R end	V [kV]	r [Ω]	l [mH]	c [μF]	g [nS]
1	8	4	230	5.29	119.27	0.88	0
2	8	5	230	8.99	129.10	0.79	0
3	4	7	230	16.93	225.92	1.53	0
4	5	9	230	20.63	238.55	1.80	0
5	7	6	230	4.50	101.03	0.75	0
6	9	6	230	6.30	141.44	1.05	0

(*) r is the total longitudinal resistance, l is the total longitudinal inductance, c is the total transversal capacitance, g is the total transversal conductance

TABLE 7. Sicilian network (102-bus system): aggregated data.

Number of buses	102
Number of PV buses	13
Number of PQ buses	85
Number of lines	75
Total line extension [km]	1930
Line voltage levels [kV]	150 220 400
Number of two-winding transformers	47
Number of three-winding transformers	4
Number of reactive shunts	10

B. APPENDIX B

Although any power flow solver can be run for PFPD-D, in this paper, PDPF [30] has been exploited. The basics of PFPD [30] are briefly presented.

PFPD is a power flow solver entirely based on a matrix approach only exploiting the nodal admittance matrix.

Given a power system network with n nodes, the relationship between the entering currents ($\underline{\boldsymbol{i}}_{\mathbf{N}}$) and the voltages ($\underline{\boldsymbol{e}}$) at its nodes can be modelled by means of its nodal admittance matrix $\underline{\boldsymbol{Y}}_{\mathbf{N}}$ ($n \times n$):

$$\underline{i}_{\mathbf{N}} = \underline{Y}_{\mathbf{N}}\, \underline{e}. \tag{A1}$$

If *all* the generators (slack and PV buses) and loads (PQ buses) are modelled as shunt admittances, a diagonal admittance matrix $\underline{\boldsymbol{Y}}_{\mathbf{SGL}}$ ($n \times n$), giving the relationship between the entering current ($\underline{\boldsymbol{i}}_{\mathbf{S}}$) into the load/generators and network voltages ($\underline{\boldsymbol{e}}$) and can be defined:

$$\underline{i}_{\mathbf{S}} = \underline{\boldsymbol{Y}}_{\mathbf{SGL}}\, \underline{\boldsymbol{e}}. \tag{A2}$$

By summing member-to-member (A1) and (A2), it is possible to write (A3), *i.e.*:

$$\underline{i} = \underline{Y}\,\underline{e}. \tag{A3}$$

where $\underline{Y} = \underline{Y}_N + \underline{Y}_{SGL}$ is the total bus admittance network admittance matrix linking the external currents injected at all network buses and the nodal voltages. This matrix is also defined as "all-inclusive" matrix, as it contains the information of all the specific power flow problem.

It is worth reminding that in PFPD the slack bus generator is modelled, for the first time in technical literature, as a current generator.

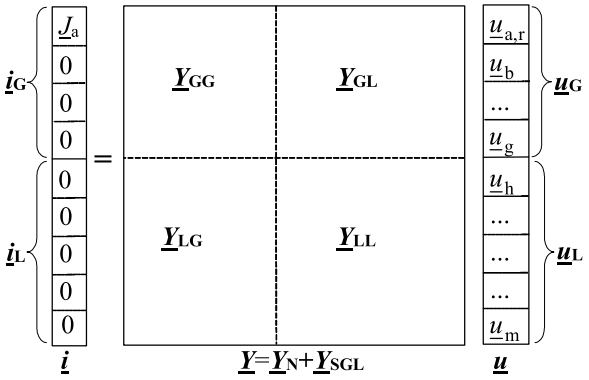

FIGURE 12. Partitioned form of $\underline{i}=\underline{Y}\,\underline{u}$.

Fig. 12 gives a graphical representation of (A3), in which it is introduced the block partition dividing generators and loads

It is worth noting that $\underline{i} = [\underline{J}_a\ 0\ 0\ \ldots 0\ 0\ 0]^t$ is the column vector of the currents injected at buses in Fig. 12.

By introducing the partition shown in Fig. 12, it follows:

$$\underline{i}_G = \underline{Y}_{GG}\underline{u}_G + \underline{Y}_{GL}\underline{u}_L \tag{A4}$$

$$0 = \underline{Y}_{LG}\underline{u}_G + \underline{Y}_{LL}\underline{u}_L. \tag{A5}$$

By applying the standard matrix procedure for variable elimination, (A5) can be rewritten as:

$$\underline{u}_L = -\,\underline{Y}_{LL}^{-1}\,\underline{Y}_{LG}\,\underline{u}_G \tag{A6}$$

The substitution of $\underline{u}_L$ in (A4) yields:

$$\underline{i}_G = \left[\underline{Y}_{GG} - \underline{Y}_{GL}\underline{Y}_{LL}^{-1}\underline{Y}_{LG}\right]\ \underline{u}_G = \underline{Y}_{Geq}\underline{u}_G \tag{A7}$$

where $\underline{Y}_{Geq}$ is the admittance matrix as seen at the generator buses. It allows, by means of its inverse, computing the impedance matrix as seen at the generator buses *i.e.*:

$$\underline{Z}_{Geq} = \underline{Y}_{Geq}^{-1} \tag{A8}$$

The element $\underline{Z}_{Geq}(1,1)$ of this matrix is the impedance as seen at slack bus and can give the current source $\underline{J}_a$ by means of:

$$\underline{J}_a = \underline{u}_{a,r} \Big/ \underline{Z}_{Geq}\,(1,\,1) \tag{A9}$$

From the computation of the matrix equations (A4)-(A9), the power flow of the entire system is determined.

However, since all the voltage phasors (except the slack voltage) are unknown, (A4)-(A9) are computed starting from a reasonable power flow initial guess (flat start), and the convergence of the power flow solution is then found iteratively.

The solution update is based on the correcting current method: suitable currents are injected into the network buses, in order to adjust the nodal voltages, which are the actual solutions of the power flow problem. Please refer to [30] for the detailed iterative formulation.

ACKNOWLEDGMENT

This paper is dedicated to the memory of Prof. Antonio Paolucci who had always advocated the importance of the approach developed in this study.

REFERENCES

[1] R. Marconato, *Electric Power Systems*, vol. 2, 2nd ed. San Jose, CA, USA: CEI, 2004.

[2] D. Chen, N. Zhou, C. Li, H. Guo, and T. Cui, "A dynamic power flow model considering the uncertainty of primary frequency regulation of system," in *Advances in Artificial Systems for Medicine and Education II*, vol. 2. Cham, Switzerland: Springer, 2020, pp. 425–438.

[3] R. Ramanathan, H. Ramchandani, and S. A. Sackett, "Dynamic load flow technique for power system simulators," *IEEE Power Eng. Rev.*, vol. PER-6, no. 8, p. 20, Aug. 1986.

[4] M. Okamura, Y. O-Ura, S. Hayashi, K. Uemura, and F. Ishiguro, "A new power flow model and solution methodlIncluding load and generator characteristics and effects of system control devices," *IEEE Trans. Power App. Syst.*, vol. PAS-94, no. 3, pp. 1042–1050, May 1975.

[5] J. Meisel, "System incremental cost calculations using the participation factor load-flow formulation," *IEEE Trans. Power Syst.*, vol. 8, no. 1, pp. 357–363, Feb. 1993.

[6] H. Zhang and S. Wang, "A distributed dynamic power flow algorithm for an interconnected system containing two-terminal LCC-HVDC tie-line," *IEEE Access*, vol. 9, pp. 28673–28683, 2021.

[7] R. Wang, H. Zhang, C. Li, and C. Ma, "Dynamic power flow calculation method of power system with wind power," in *Proc. 5th Int. Conf. Electric Utility Deregulation Restructuring Power Technol. (DRPT)*, Changsha, China, Nov. 2015, pp. 1987–1991.

[8] K. Wang, J. Zhou, Y. Yu, and Q. Lin, "A dynamic probabilistic load flow method considering random distribution of the unbalance power," in *Proc. China Int. Conf. Electr. Distrib. (CICED)*, Aug. 2016, pp. 1–7.

[9] P. Bie, B. Zhang, H. Li, Y. Zeng, M. Li, S. Zhao, J. Wu, G. Lu, Y. Wang, and G. Chen, "Probabilistic dynamic load flow algorithm considering static security risk of the power system," in *Proc. 5th Int. Conf. Electr. Utility Deregulation Restructuring Power Technol. (DRPT)*, Nov. 2015, pp. 746–750.

[10] H. Brown, G. Carter, H. Happ, and C. Person, "Power flow solution by impedance matrix iterative method," *IEEE Trans. Power App. Syst.*, vol. PAS-82, no. 65, pp. 1–10, Apr. 1963.

[11] R. Benato and G. Gardan, "A novel AC/DC power flow: HVDC-LCC/VSC inclusion into the PFPD bus admittance matrix," *IEEE Access*, vol. 10, pp. 38123–38136, 2022.

[12] J. Zhu, "Power flow analysis," in *Optimization of Power System Operation*. Cham, Switzerland: Springer, 2015, pp. 13–50.

[13] R. Benato and G. Gardan, "A new algorithm for multi-area power flow," *IEEE Access*, vol. 11, pp. 89921–89932, 2023.

[14] S. V. Dhople, Y. C. Chen, A. Al-Digs, and A. D. Domìnguez-Garcìa, "Reexamining the distributed slack bus," *IEEE Trans. Power Syst.*, vol. 35, no. 6, pp. 4870–4879, Nov. 2020.

[15] *Load Flow Calculations*, User Manual, DIgSILENT GmbH, Gomaringen, Germany, 2022.

[16] A. Agarwal, A. Pandey, M. Jereminov, and L. Pileggi, "Implicitly modeling frequency control within power flow," in *Proc. IEEE PES Innov. Smart Grid Technol. Eur. (ISGT-Eur.)*, Sep. 2019, pp. 1–5.
[17] X. Guoyu, F. D. Galiana, and S. Low, "Decoupled economic dispatch using the participation factors load flow," *IEEE Power Eng. Rev.*, vol. PER-5, no. 6, pp. 43–44, Jun. 1985.
[18] W. R. Barcelo and W. W. Lemmon, "Standardized sensitivity coefficients for power system networks," *IEEE Trans. Power Syst.*, vol. 3, no. 4, pp. 1591–1599, Nov. 1988, doi: 10.1109/59.192969.
[19] A. Zobian and M. D. Ilic, "Unbundling of transmission and ancillary services. I. Technical issues," *IEEE Trans. Power Syst.*, vol. 12, no. 2, pp. 539–548, May 1997, doi: 10.1109/59.589599.
[20] T. Van Cutsem, M.-E. Grenier, and D. Lefebvre, "Combined detailed and quasi steady-state time simulations for large-disturbance analysis," *Int. J. Electr. Power Energy Syst.*, vol. 28, no. 9, pp. 634–642, Nov. 2006.
[21] M.-E. Grenier, D. Lefebvre, and T. Van Cutsem, "Quasi steady-state models for long-term voltage and frequency dynamics simulation," in *Proc. IEEE Russia Power Tech*, Russia, Jun. 2005, pp. 1–8, doi: 10.1109/PTC.2005.4524400.
[22] T. V. Cutsem and C. Vournas, *Voltage Stability of Electric Power Systems*. Cham, Switzerland: Springer, 2008.
[23] Y. Liu and K. Sun, "Solving power system differential algebraic equations using differential transformation," *IEEE Trans. Power Syst.*, vol. 35, no. 3, pp. 2289–2299, May 2020.
[24] Y. Liu, K. Sun, and J. Dong, "A dynamized power flow method based on differential transformation," *IEEE Access*, vol. 8, pp. 182441–182450, 2020.
[25] M. Eidiani, "An efficient differential equation load flow method to assess dynamic available transfer capability with wind farms," *IET Renew. Power Gener.*, vol. 15, no. 16, pp. 3843–3855, Dec. 2021.
[26] P. M. Anderson and A. A. Fouad, *Power System Control and Stability*, 2nd ed. Piscataway, NJ, USA: IEEE Press, 2003.
[27] R. Benato, S. D. Sessa, G. Gardan, F. Palone, and F. Sanniti, "Experimental harmonic validation of 3D multiconductor cell analysis: Measurements on the 100 km long Sicily-Malta 220 kV three-core armoured cable," *IEEE Trans. Power Del.*, vol. 37, no. 1, pp. 573–581, Feb. 2022.
[28] F. Milano, "A Python-based software tool for power system analysis," in *Proc. IEEE Power Energy Soc. Gen. Meeting*, Jul. 2013, pp. 1–5.
[29] *Partecipazione Alla Regolazione Di Frequenza e Frequenza-Potenza*, Terna S.P.A., Italian Grid Code, Rome, Italy, 2006.
[30] R. Benato, "A basic AC power flow based on the bus admittance matrix incorporating loads and generators including slack bus," *IEEE Trans. Power Syst.*, vol. 37, no. 2, pp. 1363–1374, Mar. 2022, doi: 10.1109/TPWRS.2021.3104097.

ROBERTO BENATO (Senior Member, IEEE) was born in Venezia, Italy, in 1970. He received the Dr.Ing. degree in electrical engineering from the University of Padova, in 1995, and the Ph.D. degree in power systems analysis, in 1999. In 2011, he was an Associate Professor with the Department of Industrial Engineering, University of Padova. He is the author of 200 articles and four books, edited by Springer, Wolters Kluwer, and China Machine Press. He has been a member of the Six Cigré Working Groups (WGs), the Secretary of the Two Joint WGs, and a member of the IEEE PES Substations Committee. In 2014, he was nominated as a member of the IEC TC 120 "Electrical Energy Storage (EES) Systems" in the WG 4 "Environmental Issues of EES Systems." Currently, he is a Corresponding Member of the Cigré WG B1.72 "Cable Rating Verification Second Part." In 2018, he has been elevated to the grade of CIGRÉ Distinguished Member. He is a member of Italian AEIT.

GIOVANNI GARDAN (Member, IEEE) was born in Venezia, Italy, in 1995. He received the B.S. degree in energy engineering and the Dr.Ing. degree in electrical engineering from the University of Padova, in 2017 and 2020, respectively, where he is currently pursuing the Ph.D. degree in industrial engineering. His research interests include power systems modeling and high-voltage electrical engineering. He is a Young Member of Cigrè and AEIT.

FRANCESCO SANNITI (Member, IEEE) was born in Feltre, Italy, in 1994. He received the Dr.Ing. and Ph.D. degrees in electrical engineering from the University of Padova, Italy, in 2019 and 2023, respectively. Currently, he is a Research Fellow with the LTEE Laboratory, University of Padova. He is the coauthor of 23 scientific articles. His research interests include dynamic stability and control of power system restoration processes and low-inertia systems. Other recent activities regard the implementation of new algorithms for fault distance detection in single-ended traveling wave devices and the implementation of multi-period optimal power flow for transmission planning purposes. He is a member of Cigré and AEIT.

Open Access funding provided by 'Università degli Studi di Padova' within the CRUI CARE Agreement